Nature Environment and Pollution Technology
An International Quarterly Scientific Journal

p-ISSN: 0972-6268
(Print copies up to 2016)
e-ISSN: 2395-3454

Vol. 25 | No. 1 | Article ID B4328 | 2026

Original Research Paper

https://doi.org/10.46488/NEPT.2026.v25i01.B4328

Open Access Journal

# Air Aware IoT: Low-Cost Sensor Solutions for Urban Pollution Monitoring and Public Health

**K. Venugopala Rao[1], Ch. Mani Kumar[1]†, V. Saritha[2] and B. Kanthamma[3]**

[1]Department of Physics, GITAM Deemed to be University, Visakhapatnam-530045, Andhra Pradesh, India
[2]Department of Environmental Science, GITAM Deemed to be University, Visakhapatnam-530045, Andhra Pradesh, India
[3]Department of Electronics and Communication Engineering, Visakha Institute of Engineering & Technology, Visakhapatnam–530027, Andhra Pradesh, India.
†Corresponding author: Ch. Mani Kumar; mchimpin@gitam.edu

**Abbreviation: Nat. Env. & Poll. Technol.**
**Website: www.neptjournal.com**

*Received:* 26-03-2025
*Revised:* 19-05-2025
*Accepted:* 25-05-2025

*Key Words:*

Air pollution and human health
Urban air quality monitoring
Public awareness of air quality
Environmental surveillance systems
IoT-enabled air quality monitoring
Affordable pollution monitoring solutions

*Citation for the Paper:*

Rao, K.V., Mani Kumar, C., Saritha, V. and Kanthamma, B., 2026. Air aware IoT: low-cost sensor solutions for urban pollution monitoring and public health. *Nature Environment and Pollution Technology*, 25(1), B4328. https://doi.org/10.46488/NEPT.2026.v25i01.B4328

*Note: From 2025, the journal has adopted the use of Article IDs in citations instead of traditional consecutive page numbers. Each article is now given individual page ranges starting from page 1.*



## ABSTRACT

Air pollution, especially in cities, has a considerable impact on human health and contributes to global morbidity and mortality rates. With urban populations increasing and public awareness of air quality being low, there is an urgent need for low-cost portable devices to monitor airborne contaminants in indoor and outdoor settings. This study presents the design and functionality of a low-cost, portable device capable of measuring major air quality parameters, such as gaseous pollutants ($CO_2$, $O_3$, TVOC, and $PM_{2.5}$) and physical indicators (i.e., temperature and humidity). The device connects various sensors to an ATmega microcontroller via a signal conditioning circuit, thereby solving current, format, and speed incompatibilities. The data processed by the microcontroller was sent to various devices using IoT technology. The device accurately measures ozone and $PM_{2.5}$, temperature, and humidity with precisions of ±5.02 $\mu g.m^{-3}$, ±7.94 $\mu g.m^{-3}$, ±0.67°C, and ±1.68%, respectively. The results demonstrate the dependability of the system for air quality monitoring, providing an affordable and accessible alternative for environmental surveillance. This innovation has the potential to raise public awareness and enable large-scale pollution monitoring, making it a useful tool for minimizing the negative consequences of air pollution on public health.

## INTRODUCTION

Air pollution poses a significant threat to global public health, which is exacerbated by rapid urbanization and industrial growth (Kortoçi et al. 2022). Urban areas, characterized by dense populations, transportation networks, and industrial activities, are particularly vulnerable to elevated pollutant levels. Globally, air pollution contributes to over 7 million premature deaths annually due to respiratory diseases, cardiovascular disorders, and lung cancer, with 90% of the world's population exposed to pollutant concentrations exceeding the World Health Organization (WHO) guidelines (Jiang et al. 2016, Meo et al. 2021). These alarming statistics underscore the need for robust air quality monitoring systems to inform policy reforms and mitigate health risks (Perillo et al. 2022).

Existing regulatory monitoring networks, although critical, are often limited in spatial coverage and cost, restricting their deployment to specific urban zones (Baca-López et al. 2021). To address this gap, recent studies have emphasized the integration of low-cost sensors with traditional networks to enhance spatial resolution and data accessibility, particularly in underserved areas (Motlagh et al. 2021, Shindler 2021). However, conventional monitoring systems face challenges such as high power consumption, complex circuitry, and frequent calibration requirements, limiting their practicality for widespread deployment (Castell et al. 2013, Idrees et al. 2018).

Among these pollutants, particulate matter ($PM_{2.5}$) and ground-level ozone ($O_3$) are particularly hazardous because they can penetrate deep into the respiratory system and exacerbate conditions such as asthma and cardiovascular disease (Meo et al. 2021). $PM_{2.5}$ exposure is linked to elevated mortality rates, especially among vulnerable populations such as pregnant women and the elderly, whereas tropospheric ozone formed through reactions between vehicle emissions and sunlight poses severe risks in both indoor and outdoor environments (Cao & Thompson 2016). These health impacts necessitate affordable and portable devices capable of real-time multi-parameter monitoring to complement the existing infrastructure.

Recent advancements in IoT-enabled devices have shown great potential for enhancing air quality monitoring. However, many systems remain confined by low sensor precision, single-parameter concentration, and reliance on bulky or resource-bound hardware. For instance, wireless networks using ATmega328P microcontrollers have been deployed for indoor air quality monitoring but face memory constraints (Abraham & Li 2014), whereas mobile applications for outdoor pollution tracking often lack precision (Kodali & Sarjerao 2018). More recent advances, such as the IoT-based APM box, which incorporates machine learning to improve the calibration of low-cost sensors such as MQ-7 and MQ-131, provide greater pollutant measurement reliability (Rathnayake et al. 2024). Bidirectional Long Short-Term Memory (Bi-LSTM) models optimized with metaheuristic algorithms such as the Osprey Optimization Algorithm (OOA) have shown promising results for accurate $PM_{2.5}$ concentration estimation when paired with meteorological data (Saminathan & Malathy 2024). However, extensive calibration and environmental validation are required to ensure the wider applicability of these technologies.

This study aimed to design and validate a low-cost, portable, multi-sensor IoT device for real-time air quality monitoring in urban areas. To achieve this, a compact system was developed using a Raspberry Pi and an ATmega microcontroller to measure particulate matter ($PM_{2.5}$), ozone ($O_3$), total volatile organic compounds (TVOC), carbon dioxide ($CO_2$), temperature, and humidity. Although the primary emphasis of the system is on effective hardware integration, it presents a practical and scalable solution by strategically combining multiple low-cost sensors into a compact, portable, and IoT-enabled device. A custom signal conditioning circuit was implemented to address sensor incompatibilities, and Python-based software with IoT connectivity enabled real-time data visualization on both local and remote devices. Its novelty lies in the synergistic integration of diverse sensors for comprehensive air quality monitoring, real-time data transmission for accessible urban deployment, and adaptability for use across various environmental settings. This approach offers a scalable and cost-effective solution to address spatial coverage limitations in urban air quality monitoring, making it particularly suitable for city-wide deployment and community-based environmental tracking.

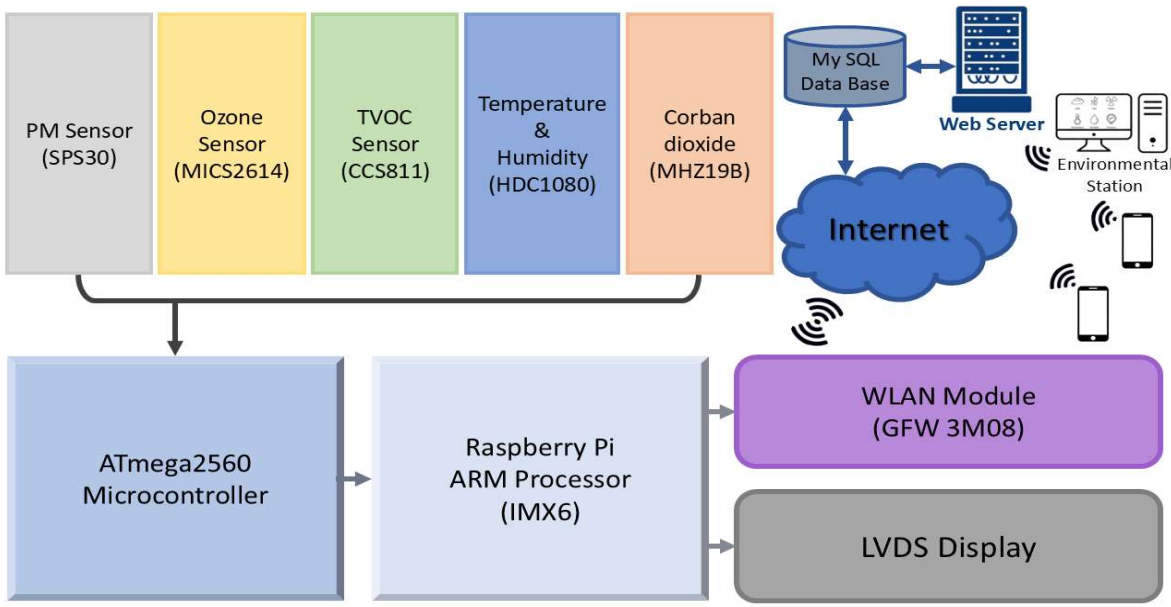


Fig. 1: Block diagram of a Portable device for measuring indoor and outdoor Air pollutants.

## MATERIALS AND METHODS

### Instrumentation

The hardware architecture of the system includes a processing unit with a Raspberry Pi, an ATmega microcontroller, and other critical components, as shown in Fig. 1. The sensors used in the sensing unit are listed in Table 1. Fig. 2 depicts the physical implementation of the portable device, emphasizing its compact and modular architecture. Fig. 3 depicts the data transmission process from the device to IoT-enabled platforms, highlighting their seamless connectivity and real-time monitoring capabilities.

To allow portability and outdoor use, the system was powered by a 5V USB supply, typically via a rechargeable power bank or wall adapter. It consumes approximately 350-400 mA during continuous operation, thereby enabling several hours of uninterrupted monitoring. As shown in Fig. 2, all the internal components are housed within a compact plastic enclosure. Although not industrially ruggedized, the casing provides basic protection against dust, light moisture, and handling, making it suitable for short-term urban and semi-outdoor deployments.

The sensing unit of the system incorporates various sensors, including the MICS 2614 ozone sensor, SPS30 particulate matter sensor, CCS811 TVOC sensor, MHZ19B $CO_2$ sensor, and HDC1080 temperature and humidity sensor. The system processing layer comprises an ATmega microcontroller(Al-Kofahi et al. 2019) and a Raspberry Pi (Vivek et al. 2017). Using these protocols, the ATmega microcontroller reads the sensor data through the signal conditioning circuit and processes the information.

The Raspberry Pi can run a software stack comprising an operating system, web server, database, and programming language. It has an execution speed of up to 1.2 GHz and can run operating systems such as Android and Linux. The communication layer of the system contains a WLAN module linked to the processor to transmit the sensor data to various IoT-enabled devices. The data analysis layer of the system displays the environmental parameters on a low-voltage differential signaling (LVDS) monitor and stores them in a database.

Most sensors used in this system provide factory-calibrated digital outputs, eliminating the need for manual calibration. The system uses temperature compensation and CRC-based checksum verification to achieve real-time software-level validation to guarantee data integrity, as shown in the software flow diagram (Fig. 4). The performance of the prototype was evaluated by placing it at a site where an Andhra Pradesh Pollution Control Board (APPCB) monitoring station was already in place. The

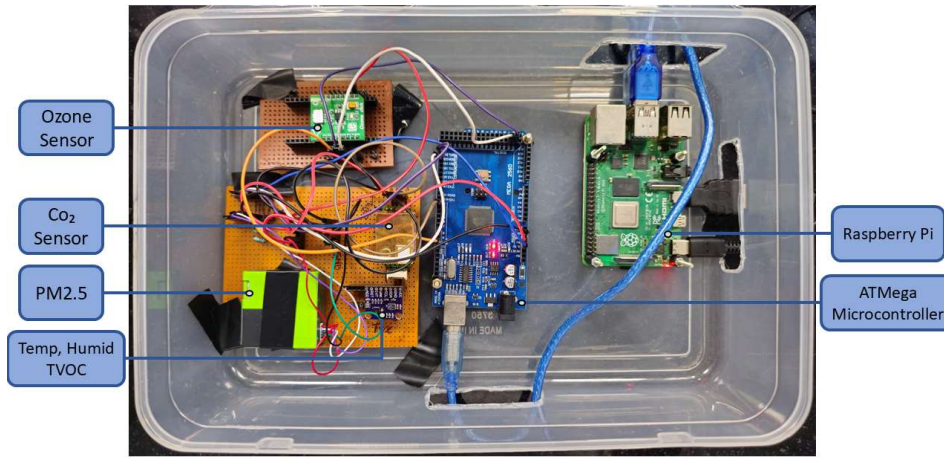


Fig. 2: Hardware Setup for a Portable Environmental Monitoring System.

Table 1: Sensors used in the sensing unit.

| Sensor Name | Measured Parameter | Range | Accuracy |
|---|---|---|---|
| SPS30 | Particulate Matter | 0 to 1000 $\mu g.m^{-3}$ | $\pm 10\ \mu g.m^{-3}$ |
| MiCS2614 | Ozone | 10 to 1000 ppb | -- |
| CCS811 | TVOC | 0 to 1187 ppb | ±15% |
| MHZ19B | $CO_2$ | 0 to 5000 ppm | ±50 ppm + 3% of reading |
| HDC1080 | Temperature & Humidity | -40°C to 125°C, 0% to 100% | ±0.2°C, ±2% |

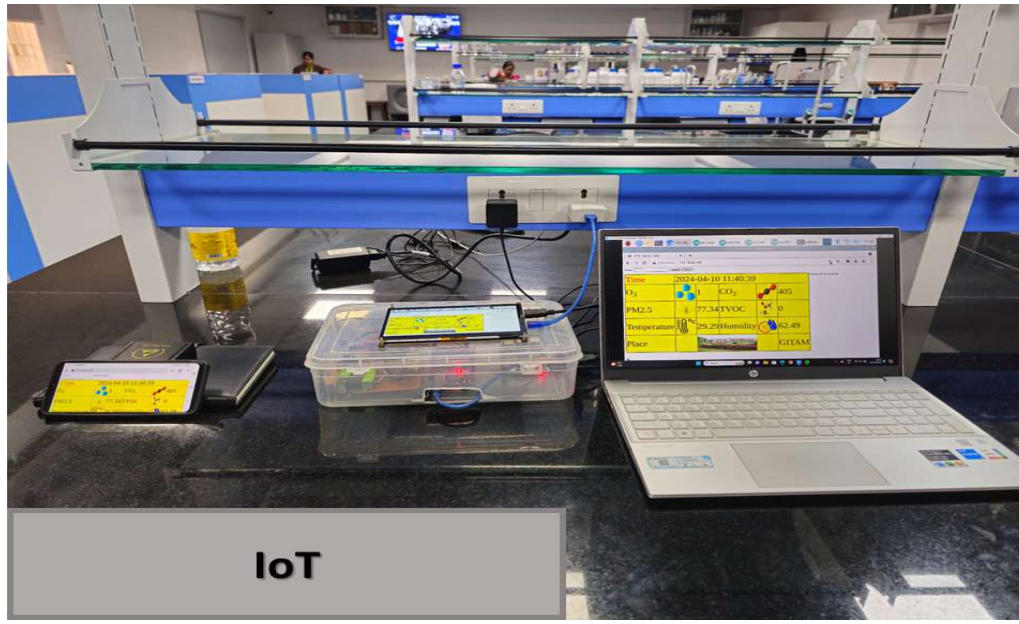


Fig. 3: Mechanism of Data Transmission to IoT Platforms.

APPCB reference values for that location were compared with the data collected by the device over 24 h. The accuracy of the system was robustly validated at the field level using statistical metrics such as Mean Absolute Error (MAE), Root Mean Square Error (RMSE), and Mean Bias (MB) to assess the results.

**Interfacing of Particulate Matter Sensor**

The SPS30 optical sensor is crucial for the precise measurement of 2.5-micrometre-diameter particles ($PM_{2.5}$) by leveraging laser scattering technology. Renowned for its stability and contamination resistance, the sensor features a built-in fan for controlled airflow regulated through an internal feedback loop. Airborne Particles passing through a laser beam generate light scattering, which is processed by algorithms on the SPS30 microcontroller, yielding an accurate mass concentration output. This comprehensive integration ensures robust performance under diverse environmental conditions.

**Interfacing of Ozone Sensor**

To monitor ozone concentrations, the MICS-2614, a MOS-type sensor, was employed with a measuring range of 10–1000 ppb. The sensor module integrates heating circuits along its edges and a sensing material. The heating circuit, powered by a voltage source, warms the sensing material by connecting the heater to the supply voltage through a resistor to form a voltage divider circuit. The MCP 3201 (ADC) operates within a voltage range of 2.7–5.5V and employs a successive approximation register (SAR) architecture. Communication between the microcontroller and ADC was facilitated using the SPI protocol. Eq. (1) is used to derive the ozone concentration from the measured ADC data.

$$\text{Ozone concentration [in ppb]} = 10^{\left(\frac{2566-(\text{ADC value}-584)}{1283}\right)} + 1 \quad \ldots(1)$$

**Interfacing of TVOC Sensor**

The CCS811 sensor, designed for measuring TVOC concentrations, integrates a microcontroller and an analog-to-digital converter. The analog output from the internal ADC was converted into a digital signal and processed by the microcontroller. Interfacing with the host microcontroller is established through the SDA and SCL pins, and operating within a current range of up to 30mA and a voltage range of 1.8 to 3.6 volts, the sensor maintains energy efficiency, consuming only 46mW.

**Interfacing of Carbon Dioxide Sensor**

An MHZ19B non-dispersive infrared (NDIR) sensor was used to monitor the ambient $CO_2$ concentration. The system consists of an infrared source, optical filter, detector, and gas chamber. The emitted infrared light closely matches the absorption band of $CO_2$, facilitating the accurate identification of $CO_2$ molecules. As light traverses the gas chamber, $CO_2$ molecules absorb specific wavelengths, and the detector measures the unabsorbed light and converts it into voltage. $CO_2$ concentration was gauged by analyzing the

on and off times of the PWM output connected to a PWM-compatible GPIO pin on the microcontroller. Additionally, the sensor was configured in the UART mode, which was connected to the transmitter and receiver pins of the controller. The on-time and off-time of the signal, extracted from the PWM output, were then substituted into Eq. (2) to derive the carbon dioxide concentration in parts per million (ppm). The integration of the PWM and UART modes enhanced the precision of the $CO_2$ measurement.

$$CO_2\ [\text{in ppm}] = \frac{Maximum\ detection\ range \times (T_{ON} - Cycle\ Start\ high\text{-}level\ output)}{T_{ON}+T_{OFF} - Cycle\ Start\ high\text{-}level\ output - Cycle\ End\ level\ output} \quad \ldots(2)$$

### Interfacing of Temperature and Humidity Sensor

The HDC1080 sensor, connected to the microcontroller through the I2C protocol for atmospheric temperature and relative humidity measurements, operates as a digital moisture and temperature sensor. Notably, this factory-calibrated sensor eliminates the need for calibration by the user. The sensor boasts high precision, with ±2% accuracy for relative humidity and ±0.2°C for temperature.

### Software Implementation

The software is responsible for controlling the different hardware devices in the system. The basic concept of embedded software is to control the operation of a group of hardware components without sacrificing their purpose or efficiency. The Raspberry Pi supports various software utilities, such as an operating system, web server, database, and scripting language for web development. In the present system, a Linux operating system is used, an Apache HTTP server is used to develop a web server, MySQL is used for database management, and the PHP scripting language is used for web development. The software implementation in this study was divided into two sections: the first was the Embedded C programming language, which was used to connect the sensors to an ATmega microcontroller. In the second section, the software stack, which runs on the Raspberry Pi, stores and distributes the data among the IoT-enabled devices. Fig. 4 shows the software implementation flowchart. The graphical user interface was built by creating PHP-scripted web pages that displayed the current environmental data and previous data stored in the database.

## RESULTS AND DISCUSSION

### Monitoring Locations and System Deployment

The system was engineered to assess air pollutant concentrations across seasons and explore variations in environmental conditions. Measurements at four locations in Visakhapatnam were compared with the Andhra Pradesh Pollution Control Board (APPCB) standards.

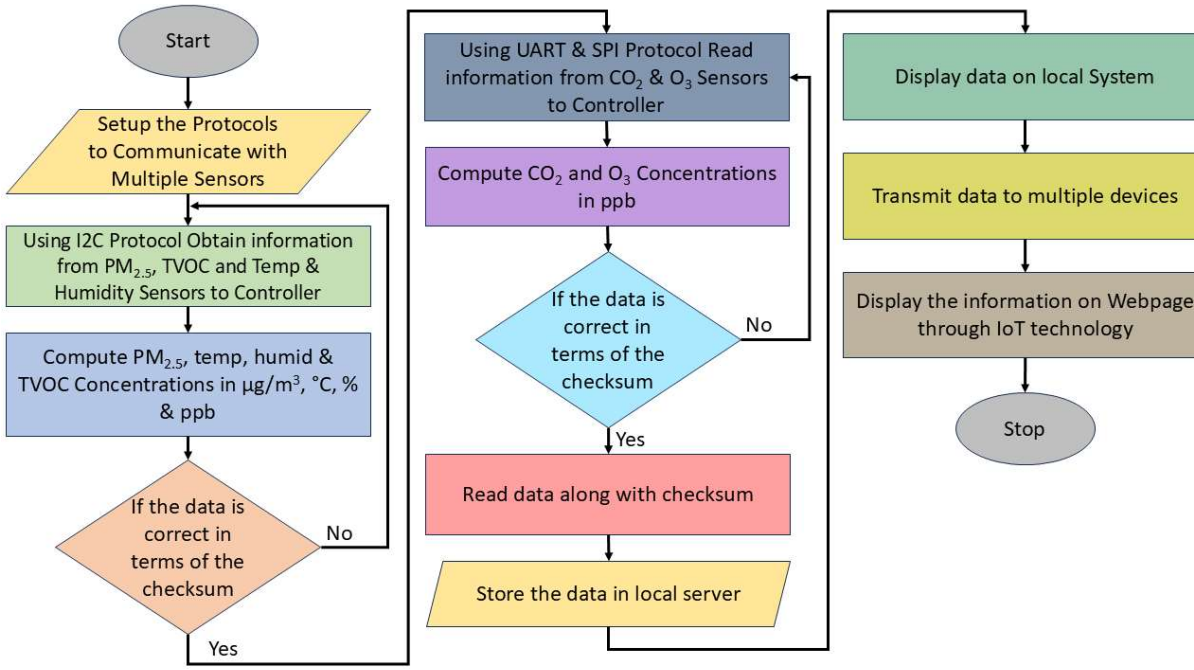


Fig. 4: Software flow diagram showing sensor communication protocols, temperature compensation, checksum validation, and IoT-based data transmission.

Continuous 24-hour measurements illuminated pollutant fluctuations in GVMC (Greater Visakhapatnam Municipal Corporation) (high population), PORT (industrial), NAD (Naval Armament Depot) (traffic), and GITAM (Gandhi Institute of Technology and Management) (green – Control Zone / Vegetative Zone). Fig. 5 illustrates the placement of the monitoring device at the GVMC and NAD locations. The system effectively measures $O_3$, $PM_{2.5}$, $CO_2$, TVOC, temperature, and humidity. The system allows for a rapid response to spikes in pollution levels. By monitoring these key pollutants and environmental conditions, the system provides valuable data for decision-makers to implement targeted interventions to improve the air quality in Visakhapatnam. This proactive approach can help mitigate the health risks associated with poor air quality and contribute to a healthier environment for urban residents. Furthermore, the collected data can be used to track trends over time and assess the effectiveness of the implemented interventions. This extensive monitoring system is essential for establishing a sustainable and healthy future for Visakhapatnam.

## Sampling and Data Collection

The prototype was deployed for 24 h at each of the four monitoring sites, GVMC, PORT, NAD, and GITAM, during each of the four seasons: summer, monsoon, autumn, and winter. This resulted in a total of 96 h of monitoring per location. Environmental data was recorded at 30-second intervals, yielding approximately 11,520 readings per sensor per site (96 h × 60 min × 2 readings per min). Data integrity was ensured through checksum validation during the data acquisition process. No additional filtering or smoothing techniques were used. The validated data were then aggregated into hourly averages to align with the standard reporting intervals, enabling seasonal trend analysis and comparison with the APPCB reference data. A summary of the seasonal deployment, sampling strategy, and preprocessing steps is provided in Table 2.

## Quantitative Error Analysis

The accuracy of the developed system was evaluated across various monitoring sites using statistical metrics, including the Mean Absolute Error (MAE), Root Mean Square Error (RMSE), and Mean Bias (MB). As shown in Table 3, the average values of $O_3$, $PM_{2.5}$, Temperature, and Humidity remained within acceptable limits, confirming the system's capability of consistent air quality monitoring. MAE values across pollutants were uniformly low, with minimal RMSE and bias, reflecting robust and precise sensor performance.


Fig. 5: The system was placed at NAD and GVMC locations in Visakhapatnam.

Table 2: Summary of Sampling and Pre-processing.

| Location | Seasons Covered | Monitoring Duration | Sampling Frequency | Total Readings (per sensor) | Data Aggregation | Pre-processing Techniques |
|---|---|---|---|---|---|---|
| GVMC PORT NAD GITAM | Summer, Monsoon, Autumn, Winter | 384 hours (24 h x 4 Seasons x 4 Locations) | Every 30 seconds | 11,520 | Hourly averages | Checksum validation only |

Table 3: Average MAE, RMSE, and MB values for $O_3$ and $PM_{2.5}$, Temperature, and Humidity across all monitoring locations.

| Location | MAE | | | | RMSE | | | | MB | | | |
|---|---|---|---|---|---|---|---|---|---|---|---|---|
| | $O_3$ | $PM_{2.5}$ | Temp. | Humidity | $O_3$ | $PM_{2.5}$ | Temp. | Humidity | $O_3$ | $PM_{2.5}$ | Temp. | Humidity |
| GVMC | 0.719 | 2.480 | 0.540 | 0.342 | 0.636 | 3.667 | 0.595 | 0.055 | -0.636 | -3.667 | -0.190 | 0.050 |
| PORT | 1.091 | 3.500 | 0.312 | 0.772 | 0.273 | 6.500 | 0.370 | 0.487 | 0.092 | -6.500 | 0.145 | -0.487 |
| NAD | 0.758 | 1.973 | 0.367 | 0.312 | 0.607 | 1.857 | 0.530 | 0.387 | -0.607 | -0.357 | -0.380 | -0.387 |
| GITAM | 1.134 | 2.417 | 0.382 | 1.080 | 0.878 | 1.885 | 0.448 | 0.715 | 0.633 | -1.115 | -0.412 | 0.440 |

Locations such as GVMC and NAD exhibited balanced metrics across all parameters, whereas PORT recorded higher $PM_{2.5}$ error, suggesting the presence of localized variability. Despite these differences, the system consistently produced accurate and reproducible measurements at all sites, demonstrating its suitability as a low-cost and scalable solution for urban environmental monitoring.

## Correlation Analysis and Observations

**Ozone dynamics: A spatial and temporal analysis:** Throughout this study, the prototype was strategically positioned at four distinct locations, each corresponding to a unique season. Continuous measurements were meticulously conducted for a comprehensive 24-hour period. The collected data were then meticulously compared with the benchmarks established by the Andhra Pradesh Pollution Control Board (APPCB), India.

Higher $O_3$ levels were recorded at the three sampling sites: GVMC, PORT, and NAD. Although the values were higher than those in other seasons, they were within the limits, as sampling was done during the COVID-19 pandemic, when human and industrial activities were restricted. Higher concentrations of ozone can be attributed to localized pollutant emissions (Mohtar et al. 2018), whereas lower concentrations at GITAM are attributed to the dispersion of pollutants due to sea breezes (Latif et al. 2012). Although $O_3$ is not a primary pollutant, its formation is triggered by oxides of nitrogen and hydrocarbons when they react with sunlight. Owing to the tropical zone, the $O_3$ concentrations were recorded to be as high as 60 $\mu g.m^{-3}$. Nitrogen dioxide is an essential factor that influences the daily variations in $O_3$. The higher concentrations of $O_3$ during the late afternoon hours are attributed to the long daylight hours (Lv et al. 2022).

Fig. 6 presents Pearson's correlation analysis, highlighting linear positive relationships ranging from moderate to very high between the measured and standard ozone levels across the four locations and seasons. The heat map visually

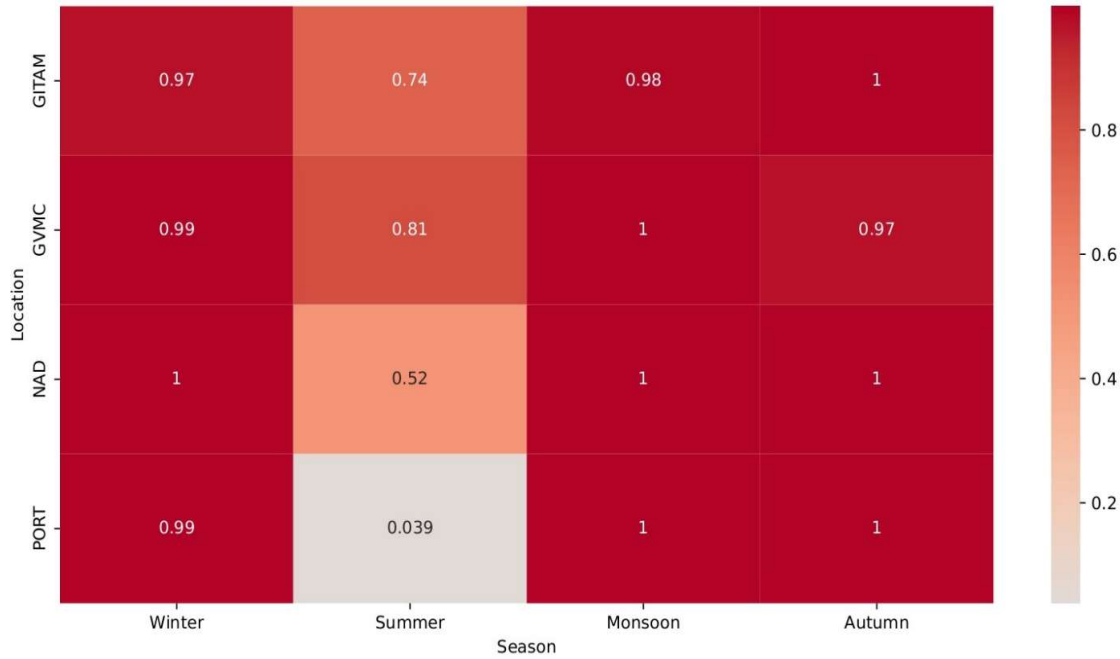


Fig. 6: Pearson Correlation of Seasonal Ozone Levels in Four Urban Locations.

depicts the correlation coefficients, showcasing the degree of correlation between the concentrations recorded by the developed system and the APPCB standards. The color intensity reflects the strength of these correlations, with values close to 1 indicating a strong positive relationship. This graph offers a concise overview of the seasonal consistency and reliability of the ozone measurements at each location.

The analysis revealed a consistently high correlation across most seasons and locations, indicating a strong alignment between the measured and standard $O_3$ levels. During the winter season, the correlations at all test locations were exceptionally high, ranging from 0.97 to 1. This suggests that the $O_3$ levels were almost perfectly aligned with the standards, reflecting reliable monitoring and stable environmental conditions. GVMC and NAD had reasonable correlations of 0.81 and 0.52, respectively, but the PORT location had a significantly low correlation of only 0.039. This rapid decline is most likely due to measurement errors. The monsoon season returned to significant correlations across all locations, with values approaching or equal to one, indicating that the measurements captured $O_3$ levels well during this period. This suggests that the accuracy of the measurements improved during the monsoon season, possibly because of less variability in the environmental factors. Overall, the data indicate that $O_3$ levels are more reliably captured during the monsoon season than during other times of the year.

**$PM_{2.5}$ dynamics: A spatial and temporal analysis:** The peak emission of particulate matter was noted between 6 AM and 12 PM and 12 PM and 6 PM near the GVMC during the Monsoon season. This diurnal variation is due to human activities, specifically vehicular movement by the population to work and businesses. $PM_{2.5}$ formed due to combustion is more hazardous as it can reach the lungs and bloodstream owing to its smaller dimensions. Changes in human activities have a significant impact on the differences in the concentration of air pollutants at various times of the day.

Fig. 7 visually represents the results of the bivariate correlation analysis, illustrating the dispersion between the concentrations measured by the developed system and the standard set by the APPCB. The Pearson correlation coefficient (r) values for the GVMC area ranged from 0.98 (winter) to 0.81 (autumn), indicating a robust and positive linear relationship. The PORT area coefficients varied from 0.92 (winter and monsoon) to 0.79 (summer and autumn), indicating a substantial correlation. NAD area exhibited correlations ranging from 0.98 (winter) to 0.92 (monsoon), underlining a commendable association. Similarly, the GITAM area demonstrated strong correlations, ranging from 0.99 (winter) to 0.89 (summer). These correlations demonstrate the effectiveness of the system in accurately capturing variations in $PM_{2.5}$ concentrations across different seasons and locations.

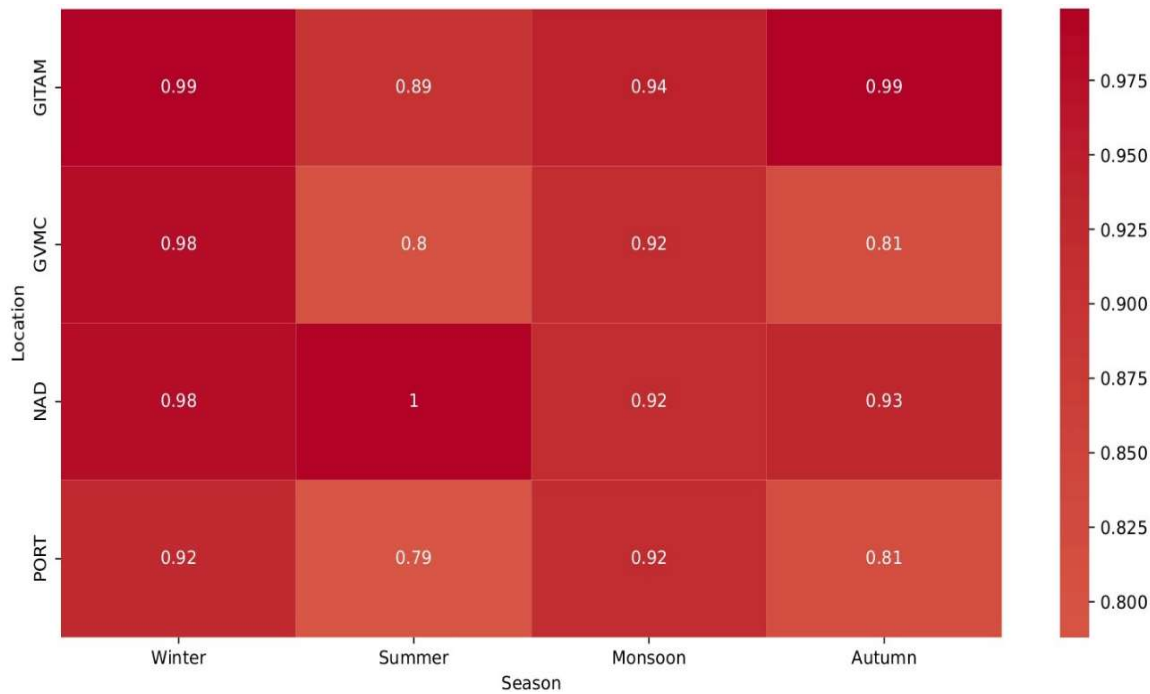


Fig. 7: Pearson Correlation of Seasonal $PM_{2.5}$ Levels in Four Urban Locations.

**Temperature and humidity dynamics: A spatial and temporal analysis:** GITAM had the lowest winter temperatures, most likely because of its green surroundings, which encourage cooling via flora. In contrast, the highest temperatures were recorded in the PORT region, which was ascribed to industrial activity that generated significant heat. Summer temperatures have increased in the GVMC, a densely populated area with significant urban heat island effects. During the monsoon, PORT and NAD had the highest temperatures, which were affected by industrial pollutants from PORT and heavy traffic on NAD. In the fall, the PORT area had the greatest and lowest temperatures, reflecting industrial heat during the day and cooling influences near the seaside at night. The average temperature concentration over seasons was compared to APPCB standard values, with an accuracy of ±0.67˚C.

During winter, GVMC had elevated relative humidity owing to high human density and water vapor emissions,

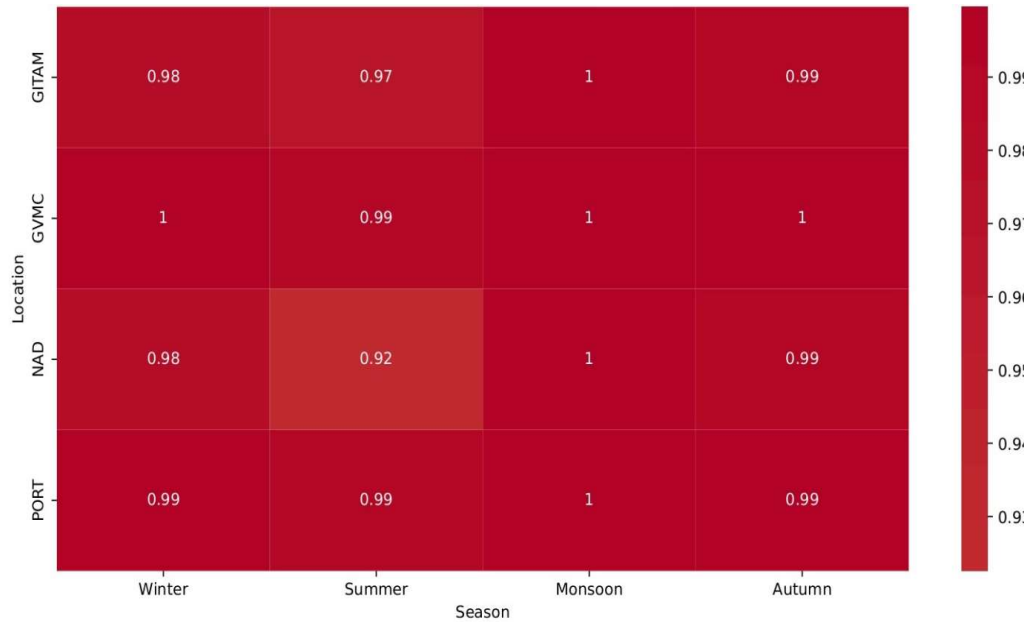


Fig. 8: Pearson Correlation of Seasonal Temperature Levels in Four Urban Locations.

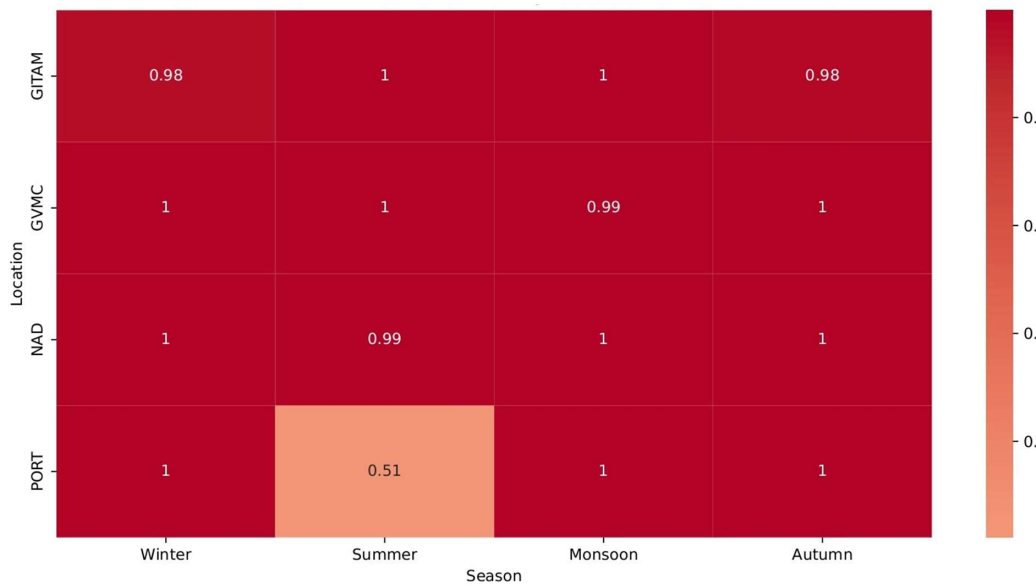


Fig. 9: Pearson Correlation of Seasonal Humidity Levels in Four Urban Locations.

whereas PORT had the lowest values, most likely because industrial heat lowered moisture. In summer, PORT had the highest humidity owing to its coastal vicinity and industrial cooling, whereas GITAM had the lowest humidity owing to its verdant surroundings and less human activity. During the monsoon, GVMC had the highest humidity, which was caused by rainfall and urban moisture retention, whereas PORT had the lowest humidity, presumably due to industrial pollutants. In autumn, GVMC again had the highest humidity owing to urban density and adjacent water sources, whereas PORT had the lowest owing to industrial heat. Across all seasons, the six-hour average humidity was compared to the APPCB requirements and achieved ±1.68% accuracy.

Figs. 8 and 9 visually portray the outcomes of the bivariate correlation analysis, showcasing the dispersion between the concentrations measured by the developed system and the standards set by the APPCB. Bivariate correlation analysis revealed strong positive relationships between the concentrations measured by the developed system and the standards set by the APPCB across all locations and seasons. In the GVMC area, the coefficients were consistently high, ranging from 0.99 to 1.00, indicating a robust correlation. Similarly, in the PORT area, the coefficients ranged from 0.99 to 1.00, indicating a strong and consistent positive correlation. In the NAD area, the coefficients showed a strong positive correlation ranging from 0.92 to 1.00. The GITAM area exhibited strong positive correlations, with coefficients ranging from 0.97–1.00 across different seasons. These findings emphasize the reliability and accuracy of the developed system for measuring pollutant concentrations under diverse environmental conditions.

In the GVMC area, a consistently strong correlation was observed across all seasons, with coefficients ranging from 0.99 to 1.00, indicating a robust agreement between the measured and standard values. The PORT area displayed a slightly lower correlation in summer (0.51), but in other seasons, it exhibited a strong correlation (1.00). Similarly, the NAD area maintained a robust correlation (1.00) across all the seasons. In the GITAM area, while maintaining a generally strong correlation, a minor decrease was observed in winter and autumn (0.98). These findings emphasize the reliability of the measurements of the developed system, which closely align with the established standards.

### Seasonal Variation of Pollutants

Pollutant concentrations were recorded to be higher during the monsoon and autumn owing to adverse meteorological conditions that would enhance the accumulation of pollutants, which can be aggravated by increased humidity (Johnson 2022, Wang et al. 2022). Previous studies have also reported that lower temperatures and wind speeds enhance particulate matter concentrations, as the meteorological conditions tend to trap these pollutants, inhibiting their outward transportation. Furthermore, higher humidity and lower temperatures favor the conversion of semi-volatile species to the aerosol phase, leading to higher concentrations of particulate matter. Our study was in line with reports confirming higher concentrations of pollutants during the monsoon and winter, along with $O_3$, since the city's average temperatures during these seasons were the same as in other seasons.

## CONCLUSION AND FUTURE WORKS

The current work presents the development of a compact air quality monitoring system built on a single-board computer and an ATmega microcontroller. The system integrates intelligent sensors to monitor $O_3$, $PM_{2.5}$, $CO_2$, TVOC, temperature, and relative humidity in both indoor and outdoor environments. Designed to be portable and cost-effective, the device operates with a 30-second sampling interval, enabling high-frequency data collection. Its IoT-enabled architecture supports real-time data transmission and remote access, making it suitable for individual use as well as community-scale monitoring. The low overall cost of the device enhances its scalability, allowing for broader deployment and improved spatial coverage in air quality assessments.

The system demonstrated consistent performance, with measurement accuracy validated against data from the Andhra Pradesh Pollution Control Board (APPCB). The observed accuracies for ozone, $PM_{2.5}$, temperature, and humidity sensors were ±5.02 $\mu g.m^{-3}$, ±7.94 $\mu g.m^{-3}$, ±0.67°C, and ±1.68%, respectively. Seasonal and spatial variations in pollutant levels were evident, with $PM_{2.5}$ concentrations notably higher during the monsoon season and peak traffic hours, highlighting the influence of both meteorological and anthropogenic factors.

While the system exhibited strong performance, certain limitations exist. The sensor accuracy under extreme temperature and humidity conditions was not extensively evaluated, and its long-term stability over several months of deployment is yet to be established. Future improvements may include weatherproofing to support extended outdoor use, integration of solar power for off-grid functionality, and cloud-based storage solutions to enable large-scale data aggregation and analysis. Additionally, the onboard Raspberry Pi presents opportunities to implement lightweight prediction algorithms capable of forecasting meteorological conditions or pollutant concentrations based on historical data. Such features could support early warning systems and enhance decision-making in environmental management.

The technology also shows significant potential for citizen science initiatives and urban-scale applications aimed at facilitating real-time, data-driven air quality interventions.

## REFERENCES


Abraham, S. and Li, X., 2014. A cost-effective wireless sensor network system for indoor air quality monitoring applications. *Procedia Computer Science*, *34*, pp.165-171.

Al-Kofahi, M.M., Al-Shorman, M.Y. and Al-Kofahi, O.M., 2019. Toward energy efficient microcontrollers and Internet-of-Things systems. *Computers and Electrical Engineering*, 79, pp.1–12.

Baca-López, K., Fresno, C., Espinal-Enríquez, J., Martínez-García, M., Camacho-López, M.A., Flores-Merino, M.V. and Hernández-Lemus, E., 2021. Spatio-temporal representativeness of air quality monitoring stations in Mexico City: Implications for public health. *Frontiers in Public Health*, 8, pp.1–15.

Cao, T. and Thompson, J.E., 2016. Personal monitoring of ozone exposure: A fully portable device for under $150 USD cost. *Sensors and Actuators B: Chemical*, 224, pp.936–943.

Castell, N., National, S., Brito, C. De and Guerreiro, B., 2013. Real-world application of new sensor technologies for air quality monitoring. *ETC / ACM Technical Paper*, 16, pp.34–45.

Idrees, Z., Zou, Z. and Zheng, L., 2018. Edge computing-based IoT architecture for low-cost air pollution monitoring systems: A comprehensive system analysis, design considerations & development. *Sensors (Switzerland)*, 18, pp.1–18.

Jiang, X.Q., Mei, X.D. & Feng, D., 2016. Air pollution and chronic airway diseases: What should people know and do? *Journal of Thoracic Disease*, 8, pp.E31–E40.

Johnson, A.C., 2022. Spatial and temporal analysis of air pollutants in Jiangsu Province, China. *Anthropogenic Pollution*, 6, pp.47–54.

Kodali, R.K. and Sarjerao, B.S., 2018. MQTT-based air quality monitoring. *5th IEEE Region 10 Humanitarian Technology Conference*, 742–745.

Kortoçi, P., Motlagh, N.H., Zaidan, M.A., Fung, P.L., Varjonen, S., Rebeiro-Hargrave, A., Niemi, J.V., Nurmi, P. and Hussein, T., 2022. Air pollution exposure monitoring using portable low-cost air quality sensors. *Smart Health*, 23, pp.1–12.

Latif, M.T., Huey, L.S. and Juneng, L., 2012. Variations of surface ozone concentration across the Klang Valley, Malaysia. *Atmospheric Environment*, 61, pp.434–445.

Lv, Y., Tian, H., Luo, L., Liu, S., Bai, X., Zhao, H., Lin, S., Zhao, S., Guo, Z., Xiao, Y. and Yang, J., 2022. Meteorology-normalized variations of air quality during the COVID-19 lockdown in three Chinese megacities. *Atmospheric Pollution Research*, 13, pp.101452.

Meo, S.A., Abukhalaf, A.A., Alomar, A.A., Alessa, O.M., Sami, W. and Klonoff, D.C., 2021. Effect of environmental pollutants PM-2.5, carbon monoxide, and ozone on the incidence and mortality of SARS-COV-2 infection in ten wildfire-affected counties in California. *Science of the Total Environment*, 757, pp.143948.

Mohtar, A.A.A., Latif, M.T., Baharudin, N.H., Ahamad, F., Chung, J.X., Othman, M. and Juneng, L., 2018. Variation of major air pollutants in different seasonal conditions in an urban environment in Malaysia. *Geoscience Letters*, 5, pp.1–9.

Motlagh, N.H., Zaidan, M.A., Fung, P.L., Lagerspetz, E., Aula, K., Varjonen, S., Siekkinen, M., Rebeiro-Hargrave, A., Petäjä, T., Matsumi, Y., Kulmala, M., Hussein, T., Nurmi, P. and Tarkoma, S., 2021. Transit pollution exposure monitoring using low-cost wearable sensors. *Transportation Research Part D: Transport and Environment*, 98, pp.102981.

Perillo, H.A., Broderick, B.M., Gill, L.W., McNabola, A., Kumar, P. and Gallagher, J., 2022. Spatiotemporal representativeness of air pollution monitoring in Dublin, Ireland. *Science of the Total Environment*, 827, pp.154299.

Rathnayake, L.R.S.D., Sakura, G.B., Weerasekara, N.A. and Sandaruwan, P.D., 2024. Machine learning-based calibration approach for low-cost air pollution sensors MQ-7 and MQ-131. *Natural Environment and Pollution Technology*, 23, pp.401–408.

Saminathan, S. and Malathy, C., 2024. PM2.5 concentration estimation using Bi-LSTM with Osprey optimization method. *Natural Environment and Pollution Technology*, 23, pp.1631–1638.

Shindler, L., 2021. Development of a low-cost sensing platform for air quality monitoring: Application in the city of Rome. *Environmental Technology (United Kingdom)*, 42, pp.618–631.

Vivek, N., Sowjanya, P., Sunny, B. and Srikanth, S.V., 2017. Implementation of IEEE 1609 WAVE/DSRC stack in Linux. *TENSYMP 2017 - IEEE International Symposium on Technology for Smart Cities*, pp.2–6.

Wang, J., Zhao, Y. and Xu, M., 2022. Distribution characteristics of six criteria air pollutants under different air quality levels in Cangzhou City, China. *Journal of Health and Environmental Research*, 8, pp.9–16.